

UWB Multi-User Interference Signal Considerations

H. Luediger & B. Kull
{luediger, kull}@imst.de
IMST GmbH, 74745 Kamp-Lintfort, Germany

Abstract. In any power-shared multi-user system it is of high importance to understand and control the mechanisms of mutual interference of system users. Due to the expected high density of autonomous UWB devices in future home, office and hot spot scenarios, the local capacity of the ‘UWB resource pool’ needs to be assessed in order to enable the development of appropriate services and applications. The presented interference models are applicable for low, medium and high UWB device densities in indoor and outdoor free-space scenarios. Depending on the number of users and the system load it is found that for many 2D UWB interferer topologies the statistics of the multi-user noise can be approximated by Gamma- or power-law distributions, respectively.

Keywords: UWB signal statistics, multi-user interference

1. Introduction

Since the adoption of WCDMA for 3G mobile communication systems, multi-user interference was discussed mainly on the basis of the ‘Gaussian’ assumption. Due to the fact that in CDMA systems a basically continuous signal is transmitted and hence many individual signals form the total interference signal at any time, the central limit theorem may be cited rightly in most cases. In impulsive UWB systems the theorem would require each ‘timeslot’ (duration of an impulse) coincidentally be used by a relatively high number of users, which is an unrealistic assumption, i.e. only at multiple capacity overload of the UWB system Gaussian interference signal statistics would prevail.

Multi-user interference statistics are driven by the distance-power law. Under free-space conditions the transmitted signal power decay is proportional to the square, or the amplitude - as primarily used in this model - proportional to the interferer distance. If sequentially observed in an infinite, uniformly distributed interferer population, the probability density of an amplitude x is

$$p(x) = \frac{c}{|x^3|}$$

for rectangular pulses of random polarity and uniform transmit peak power. It can be

derived as follows: a constant interferer density in a circular area requires the number of interferer in annuli of constant width to grow linearly with the radius r .

$$p_R(r) = c_1 r$$

Under free-space conditions the modulus of the received amplitudes x is inversely proportional to the radius r

$$x = \frac{c_2}{r}$$

and with $g(r) = \frac{c_2}{r}$

the transformation

$$p_x(x) = \frac{p(r)}{|g'(r)|}$$

yields

$$p_x(x) = \frac{c_1 r}{\frac{c_2}{r^2}} = \frac{c_1 r^3}{c_2} = \frac{c_1 c_2^2}{x^3} \quad (1)$$

The power-law nature of the distribution (1) of interference amplitudes with exponent 3 causes twofold trouble. For small amplitudes the density approaches infinity, which leads to infinite variance and necessitates the limitation of the range of amplitudes towards the lower end (equivalent to a maximum interferer distance). Also for $x \rightarrow \infty$ the variance of

the distribution is infinite. Therefore the range of amplitudes needs to be limited towards high amplitudes (minimum distance) too. Both limitations, however, are quite natural under realistic conditions.

2. Case I: Huge interferer population

The interference model is based on a uniform distribution of interferer with finite density in a circular area. Independent interferer transmit rectangular impulses with random polarity at uniform peak power levels and arbitrary pulse rates. The system load factor μ is defined as the accumulated pulse rate C_p of all interferer multiplied by τ , the maximum impulse duration

$$\mu = C_p \tau. \quad (2)$$

Case I is modelled as a very high number of interferer transmitting pulses at very low pulse rates such that the system load factor remains far below 1. At less than 5 % system load factor, collisions between individual interferer pulses are so rare that the total interference signal distribution is very well approximated by the distribution of sequentially observed (collision-free) interferer signals. Given a rectangular pulse shape and uniformly distributed interferer, the sequentially observed statistical amplitude X of the total interference signal is characterised by the random variable

$$X = \pm \frac{\text{const.}}{R} \quad (3)$$

with R being another random variable the square of which is uniformly distributed. The inverse of R is proportional to the received interferer amplitude level. According to (1) the probability density distribution of X is

$$p_X(x) = \begin{cases} \frac{c}{|x^3|}, & \frac{\text{const.}}{r_{\max}} < x < \frac{\text{const.}}{r_{\min}} \\ 0 & \text{elsewhere} \end{cases}. \quad (4)$$

The persistent nature of power-law variables as regards manipulation lets us expect only little alterations of the distribution when other than rectangular pulse shapes are employed. Two different waveforms were simulated as the product of the statistical variable X (3) and the statistical variable representing the respective pulse shape. Fig. 1 shows sequential (collision-free) amplitude histograms of a uniform interferer distribution in case i) sinusoidal mono-cycles and ii) a Gaussian “W”

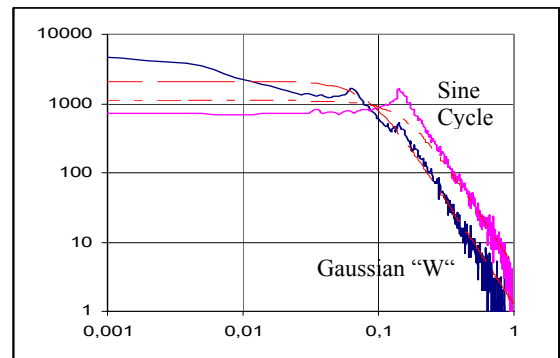


Fig.1a Sequential interference histograms at max. interferer range ratio of 1:8 (r_{\min} / r_{\max})

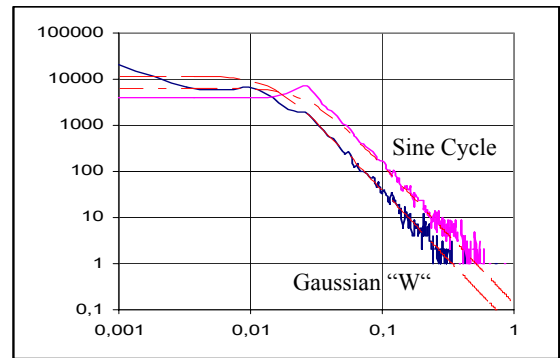


Fig.1b Sequential interference histograms at max. interferer range ratio of 1:40 (r_{\min} / r_{\max})

waveform (6) are received, respectively. High and medium amplitudes remain strictly power-law distributed whereas the density of low amplitudes ties up with the ordinate in a manner depending on the actual pulse shape. All plots have been overlaid with an approximating density distribution (scaled to histogram levels). In order to serve as a low system load (quasi collision-free) amplitude distribution, it will be used for amplitudes between positive and negative extremes and set to

zero elsewhere. The integral error introduced by the cut-off is very small if it occurs at more than approximately three orders of magnitudes below the peak probability density. The approximating density distribution is

$$p_x^A(x) = \frac{6\sqrt{3}}{8\pi} \cdot \frac{1}{\beta \left(1 + \frac{|x|^3}{\beta^3} \right)} \quad (5)$$

for

$$x = [-\infty, \infty]$$

A low system load can be affected by multiplying the clipped distribution (5) with a reduction factor $1-\alpha < 1$ followed by the introduction of the discrete zero probability α such that the total probability yields one. The discrete zero probability is equivalent to the fraction of time in which no interferer transmits a signal and is well approximated by Poisson statistics $\alpha = p_{\text{Poisson}}(0, \mu)$ for a huge number of events where μ is defined according to (2). The system load factor was set to $\mu = 0.05$, yielding a discrete zero probability $\alpha = 0.9512$ and a reduction factor $1-\alpha = 0.0488$. Under those conditions the system is considered collision-free. Then, according to the desired system load factor, the total interference signal density function can be obtained by multiple convolutions of the modified distribution with itself. Fig. 2 shows the effect of increasing system load, which can be figured as an increase either of interferer pulse rates or of the interferer density.

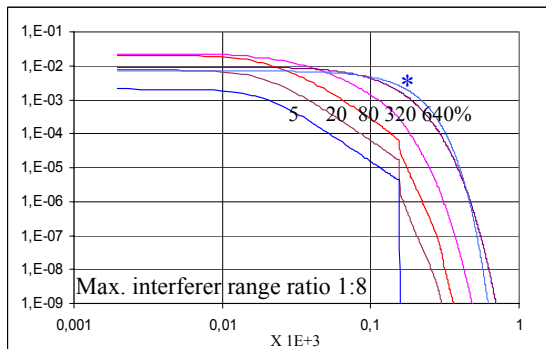


Fig.2a Distribution of interference signal at 5%, 20%, 80%, 320% and 640% system load μ

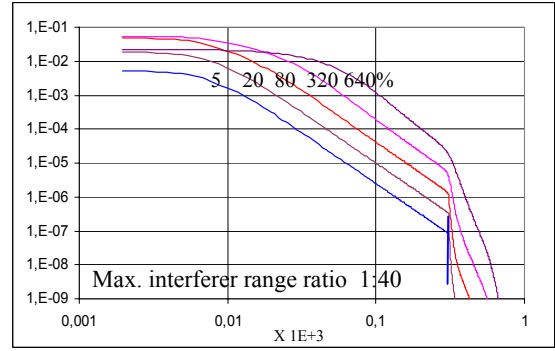


Fig.2b Distribution of interference signal at 5%, 20%, 80%, 320% and 640% system load μ

Only when a system with a maximum interferer range ratio of 1:8 (Fig.2a) is more than 6 times overloaded, the resulting density function starts to resemble a normal* distribution. The rate of convergence towards a normal distribution depends on the maximum interferer range ratio and is extremely low for high ratios, i.e. extended interferer distributions, as shown in Fig. 2b where the distance to the most remote interferer is 40 times greater than to the nearest. The apparent inequality of the areas under the distributions of Fig. 2 is caused by the changing discrete zero probability which is not shown in the plots.

3. Case II: Small and medium interferer populations

In case of very low system load factor μ and small interferer population, the interference amplitude distribution is dominated by singularities of single interferer signal distributions and often cannot be described in closed form. Hence it is difficult to derive the interference signal statistics at higher system loads, which is likely to have supported the reluctant acceptance of Gaussian UWB interference signal properties e.g. [1],[2],[3]. Two simulations were performed in order to study the interference noise more closely. The first employs a complete transmitter-receiver simulation chain [4] that was used to capture the interference signal properties at the output of a matched correlation

receiver. The received interference pulses were of the Gaussian “W” waveform, i.e. the first derivative of a Gaussian monocycle. The actual shape of the received pulse is given by (6) with $T_p = 0.2877 \text{ ns}$ and has been taken from literature [5]. The maximum simulated pulse length was $\tau = 0.859 \text{ ns}$.

$$w(t) = \left(1 - 4\pi \frac{t^2}{T_p^2} \right) \exp \left(-2\pi \frac{t^2}{T_p^2} \right) \quad (6)$$

The number of interferer was set to 17 and their position in a 5mx5m area was randomly fixed such that on the average a uniform spatial distribution of interferer, separated by more than 10 cm, was achieved. Each interferer was randomly assigned an up- or downlink of 80 Mpps to a node in the centre of the area leading to a system load factor μ of approx. 115%.

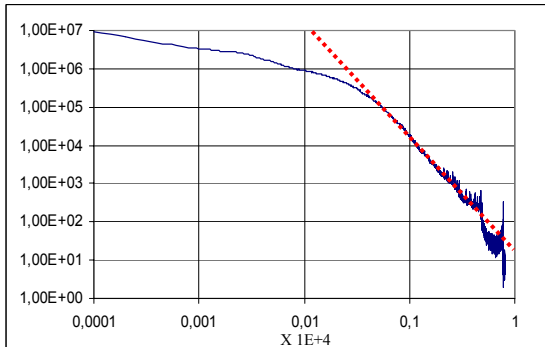


Fig.3a Mean interference histogram, Pareto opt. power control

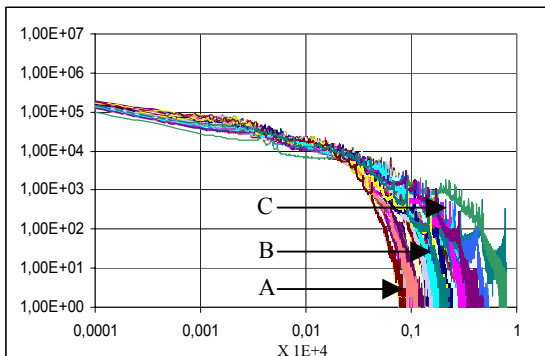


Fig.3b Individual histograms, Pareto opt. power control

The transmit power of interferer was controlled in a Pareto optimal manner [4] and the interference signal was determined at a randomly selected position in the

5mx5m area in each case. The mean (collective) interference signal histogram, built from 62 simulation scenarios, is presented in Fig. 3a and it is no surprise we find the power-law in the distribution of amplitudes (cx^{-3} inserted for reference). Though representing the collective interference histogram under Pareto optimal power control, it is far from interference histograms of individual simulation scenarios which are shown in Fig. 3b. A normal distribution was found to match neither the inclined roof nor the tail of the simulated individual distributions. Much better fits were achieved with a modified Gamma distribution for the majority of simulation results, i.e. the modulus of the interference amplitude. Similar to the high interferer density case (Case I), the Gamma distribution needs to be reduced due to the significant discrete zero probability α that prevails even in a system loaded at 2 times 115 %. The density of amplitudes greater than zero follows a Gamma distribution.

$$p_X^G(x) = \frac{(x/\beta)^{\gamma-1} \exp(-x/\beta)}{\beta \cdot \Gamma(\gamma)} \quad (7)$$

The factor 2 accounts for the correlation performed by the receiver, i.e. for the doubling of the pulse length and the system load factor. The new system load factor

$$\mu' = C_p 2\tau \quad (8)$$

reflects the signal properties at the output of the correlation receiver. Comparison of (7) with normalized histograms derived from the simulation requires double adaptation. Due to the finite amplitude bin width of the histograms obtained by simulations, the probability of the smallest amplitude bin in general is a mixture of the discrete zero-probability and the probability of very small amplitudes in that bin. The sum of the two forms a quasi zero-probability which needs to be applied when reducing (7). Figure 5 shows the effect for an extremely small bin width. In

all other plots the extremely small amplitudes have been attributed to the discrete zero probability. For coherence reasons all further load figures refer to the system load factor prior to correlation, i.e. to μ rather than μ' .

Following above procedure, the reduced distribution (7) was tested for three typical interferer topologies representing a low, medium and high interference signal variance. Those cases are indicated in Fig. 3b by the letters A through C and cover a variance range of more than two orders of magnitude. For all three cases γ was set to $2/3$ and α to 0.22 , both derived from the simulation. (Please note that the theoretical discrete zero probability α for a system load factor $\mu' = 2 \cdot 1,15$ is 0.1). The scale parameter β was adjusted for equal variance.

Figures 4a through 4c show typical interference distributions for the selected cases and the fitted Gamma distribution. In case A, the low variance case, the exponential decay underestimates the steepness of the tail of the actual distribution. This case corresponds to a scenario where interferer have similar distances to the point of observation which leads to approximately equal amplitudes of individual interferer. It is known to relatively quickly converge to a Gaussian interference signal distribution. Distributions with medium variance (case B) cover approximately $2/3$ of all cases and can be fitted best to a Gamma distribution as shown in Fig.4b. The spikes in the simulated distributions correspond to peaks in the amplitude distribution of a single strong interferer. Fig. 4c, corresponding to the presence of several near by interferer (case C), exhibits spikes of strong signals and a generally poor fit of the Gamma distribution. However, the relative frequency of occurrence of high variance scenarios is less than four percent of all cases. In order to make the modified Gamma distribution applicable for a wider range of system loads, it must be ensured

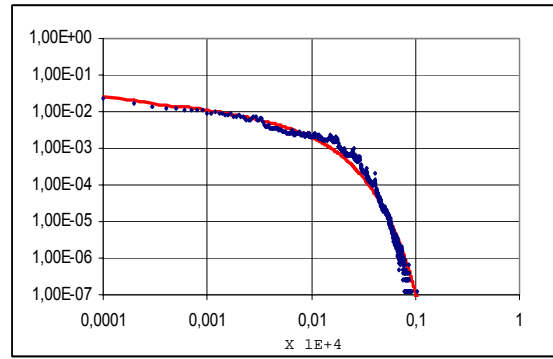


Fig.4a Simulated/fitted distributions case A

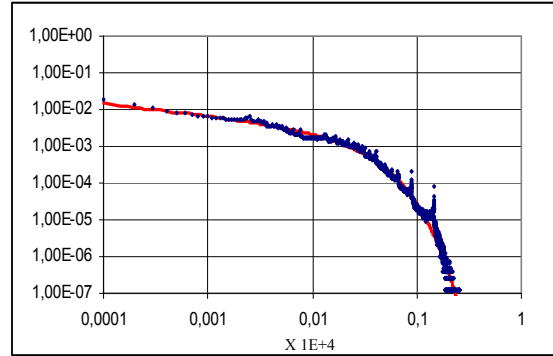


Fig.4b Simulated/fitted distributions case B

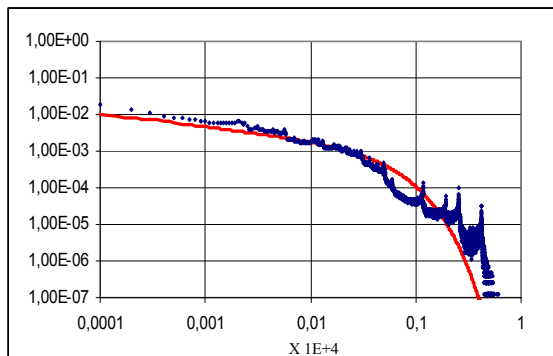


Fig.4c Simulated/fitted distributions case C

that the shape of the actual distribution remains stable, which was analysed in another simulation where the sequential interference amplitude density was constructed based on the knowledge of the common interferer pulse shape, the received power levels of the 17 interferer and the system load factor μ . The initial system load factor was chosen to be $\mu = 0.025$ (leading to $\mu' = 0.05$) and the system assumed collision-free. Different system load factors were affected by multiple convolutions and realized as the inverse Fourier transform of powers of the forward transform of the starting distribution. Results are shown in Figures 5a and 5b. In Fig. 5a, next to the starting

distribution, the distributions for 20, 80 and 115 percent system load (bottom up) exhibit a fairly stable shape of the distribution. The corresponding 115 % load factor distribution obtained from the transmitter-receiver chain simulation is indicated by red stars. The match is almost perfect and validates the methodology of extrapolating amplitude distributions at high system loads from initial quasi collision-free distributions. In Fig. 5b the

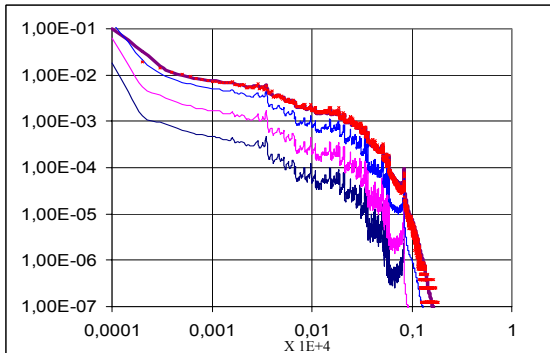


Fig.5a Distributions at 2.5, 10, 40 and 115% load

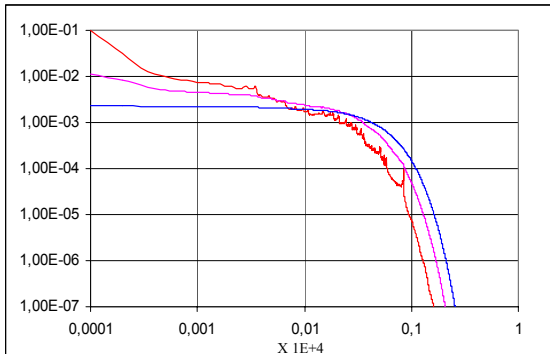


Fig.5b Distributions at 115, 320 and 640% load

system load factor μ is further increased from 115 to 320 and 640 % (ordinate top down). The sustained high degree of parallelism of the distributions at high amplitudes suggests that yet at 640 percent system load the exponential nature of the distribution dominates the developing normal distribution.

The limits of applicability of the Gamma distribution have been investigated and the extreme system load factors of the dominant type B interferer scenario were determined for which total interference distributions either degenerate to the sum of individual interferer distributions or start to develop a Gaussian character, resp.

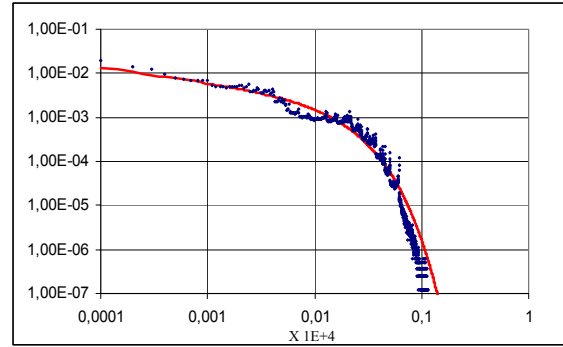


Fig.6a Type B scenario at 57.5% system load

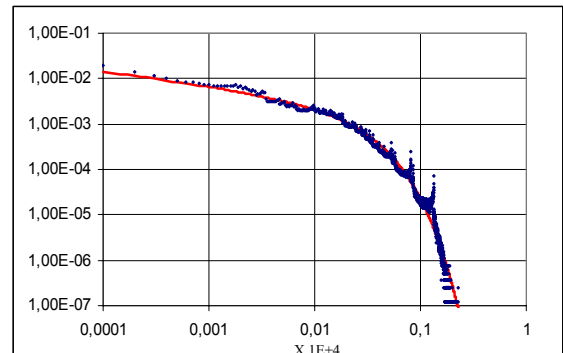


Fig.6b Type B scenario at 115% system load

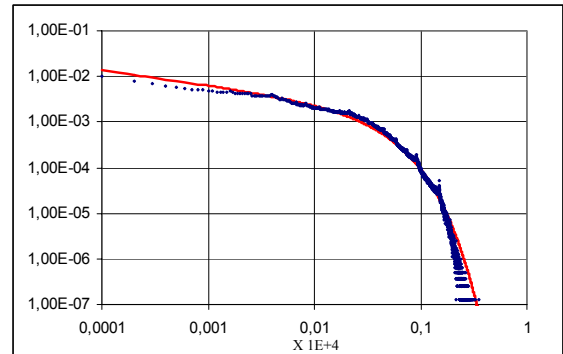


Fig.6c Type B scenario at 230% system load

Approximately below 70% and above 250% system load factor μ the Gamma distribution starts to deviate noticeably from the actual distribution, particularly at low and high amplitude levels. Figures 6a through 6c show typical interference distributions and fitted reduced Gamma distributions (red).

4. Conclusions

For huge, uniformly distributed 2D interferer populations and low cumulative data rates, e.g. in extended RFID scenarios, the total interference signal distribution was shown to be of the power-law type, which exactly holds for rectangular pulse

shapes. For other than rectangular pulse shapes a modified power-law distribution has been proposed which well approximates the amplitude density distribution of sinusoidal and Gaussian pulse shapes. It was also found that for increasing system load this kind of distribution converges only slowly to a normal distribution, i.e. only at multiple system overload a Gaussian distribution of amplitudes prevails. For smaller interferer populations a modified Gamma distribution was fitted with good results to the interference signal distribution of a power controlled system employing a Gaussian waveform and operating at low to medium loads. Only beyond system load factors of 300% the effect of increasing pulse collisions slowly transforms the Gamma- into a Gaussian distribution.

References

- [1] Yoshiyuki Ishiyama, Tomoaki Ohtsuki, Performance Analysis of UWB-IR Systems with Multiple Modulation, IWUWBS 2003, Oulu
- [2] Li Zhao, Alexander Haimovich, Multi-User Capacity of M-Ary Ultra-Wideband Communications, UWBST 2002, Baltimore
- [3] Moe Z. Win, R. A. Scholz, Ultra-Wide Bandwidth Time-Hopping Spread Spectrum Impulse Radio for Wireless Multiple Access Communications, IEEE Trans. Vol. 48, No.4, April 2000
- [4] Whyless.com project reports on UWB at <http://www.whyless.org/public/project.htm>
- [5] Moe Z. Win, On the Energy Capture of Ultrawide Bandwidth Signals in Dense Multipath Environments, IEEE Communications Letters, Vol.2, No.9, September 1998